

## Three-Dimensional Analysis of the Thermal Behavior of Alumina-Water Nanofluid Inside Hexagonal and Octagonal Enclosed Domain

Zainab Kareem Ghoben<sup>1,2,\*</sup>, Ahmed Kadhim Hussein<sup>2</sup>

<sup>1</sup> Ministry of Agriculture, Planning Department, Al-Diwaniya, Iraq

<sup>2</sup> University of Babylon, College of Engineering, Mechanical Engineering Department, Babylon City, Hilla, Iraq

### ARTICLE INFO

### ABSTRACT

#### Article history:

Received 25 August 2022

Received in revised form 5 January 2023

Accepted 13 January 2023

Available online 1 February 2023

#### Keywords:

Hexagonal; octagonal; three dimensional; cavity; nanofluid

The current work focused on the study of the laminar and steady free convection of Aluminum Oxide / Water nanofluid inside cavities. Two different cavities have the same volume but different overall surface area and count of walls are studied. These cavities are heated differentially on the vertical square side walls which of identical area and dimensions for both cavities. The other vertical walls of these cavities have hexagonal and octagonal shapes. The first cavity has eight walls while the second has ten walls. The study accomplished for solid particles volume fraction and Rayleigh number ranges of ( $\phi = 0.01, 0.03, 0.05$ ) and ( $10^3 \leq Ra \leq 10^6$ ). The study interested highly by the effect of the cavity geometry parameters including the lateral cross section, the height, the number of walls on the flow and heat transfer. Other flow parameters are recognized on the fluid flow and heat transfer fields like the nanoparticles volume fraction and the Rayleigh number. The results indicated that the surface area increase by means the additional walls has an observed effect on guiding the results. Where the octagonal cavity has better enhancement in heat transfer especially at ( $Ra=10^4$  and  $10^5$ ). The percent increase in Nu over the hexagonal cavity is (0.6, 0.8, 0.7, 0.3) for the specified Ra range.

## 1. Introduction

The configuration of the enclosure which contains the free convection of different nanofluids in three-dimensional (3D) were the specific field that interested by this work. In the last decays the heat transferred by free convection inside enclosures were gained a great interest because of its wide engineering applications. Different configurations of enclosures and working fluids are investigated numerically and experimentally [1-5]. Different geometries of the cavities; cubical or non-cubical are discovered [5-8]. The various shapes of cavities are discovered for many conditions to enhance the heat transferred. The techniques are changing the shape and/or the inclination of the cavity [9-13]. Equipping the cavity with fins is another technique to enhance the convection heat inside [14,15]. The fins are of different shapes and locations and fabricated as rigid or sometimes porous [16-19]. Enhancing the properties of the working fluids by means of (Ra) range is also considered [20-23]. In

\* Corresponding author.

E-mail address: [zainabghoben@gmail.com](mailto:zainabghoben@gmail.com)

<https://doi.org/10.37934/arfmts.103.1.4063>

the recent years, the researchers depending on the fluid additives which is an effective idea. The classical fluids like water, oil and else are loaded with metallic or ceramic nanoparticles to enhance the thermal abilities [24-31]. By time the researches approved that these properties are approved by specific volume fraction range of nanoparticles ranging around ( $0 \leq \varphi \leq 0.06$ ) [32-34]. The range is optimum to satisfy the desired enhancement with avoiding agglomeration and dissipation of the solid phase [35]. The magnetization of the field is also used to enhance the convection inside cavities [36]. It is very important in many industrial applications like casting [37-39]. The porous media is also promising technique which depends on by some researchers in building their enclosures [40-42].

In the present work, the three-dimensional cavities with different configurations and filled with nanofluid are interested in. In classical (cubical) cavities that heated differentially, Kolsi *et al.*, [43] enclosure filled with  $\text{Al}_2\text{O}_3$ -water while Salari *et al.*, [44,45] enclosure filled by air and MWCNT-water. Then, adding fillets to the cavity and repeating their study [45]. Whereas, Kolsi *et al.*, [46] cavity containing twin adiabatic blocks and filled with  $\text{Al}_2\text{O}_3$ -water. Kolsi *et al.*, [47] cavity having triangular cross section solid baffles at corners. Three cases were studied for counts and positions of the inserts. Kolsi *et al.*, [48] cavity is open and containing an adiabatic diamond obstacle. Then, Kolsi *et al.*, [46] supplies the top surface to the gas above. While the magneto free convection inside the opened cavity with an attached inclined plate and filled with CNT-water is accomplished by Kolsi *et al.*, [49]. Rahimi *et al.*, [37] working fluid is the CuO-water nanofluid while the seawater and  $\text{Al}_2\text{O}_3$  nanoparticles with magnetic field effect are discovered by Jelodari and Nikseresht [50]. Al-Rashed *et al.*, [14] cavity is inclined containing conductive Ahmed body at the center and filled with CNT-water. While, Al-Rashed *et al.*, [15] examined the entropy field. Moutaouakil *et al.*, [51] cavity is filled of different water based nanofluids (Cu,  $\text{Al}_2\text{O}_3$ , Ag,  $\text{TiO}_2$ ). It is heated by three parallel and identical elements for different inclinations. As like as others, Sannad *et al.*, [52] cavity is designed also to understand the effect of the same water based nanofluids but for only three type of nanoparticles ( $\text{Al}_2\text{O}_3$ , Cu and  $\text{TiO}_2$ ) nanoparticles. Then examine other heating manner of cavity using a hot partition of uniform temperature instead of partially manner [53]. Esfe *et al.*, [38] equipped the cavity that filled by CuO-water with porous fins. For non-cubical enclosures, in rectangular with one inclined hot sidewall and inclined inner of T-shape as additional heat source Selimefendigil and Öztöp [54] discovered the field. While Al-Rashed *et al.*, [55] cavity is of parallelogrammatical configuration and occupied by CNT-water. It was with partially heated square at the bottom side. The top side is opened and filled  $\text{Al}_2\text{O}_3$ -water in Al-Rashed *et al.*, [16] study. Bendrer *et al.*, [56] cavity is wavy cubical with rectangular heated area located at the bottom. The flow is divided into two layers porous and hybrid nanofluid. The current study is focused on two different configurations of the 3D cavities filled with  $\text{Al}_2\text{O}_3$ -water nanofluid and the effects on the heat transfer enhancement. The first has eight walls and hexagonal front cross section. While the other has ten walls and octagonal front cross section.

## 2. The Geometry

In this work, two enclosures are designed where the left and right walls are squares while the front and back walls are hexagonal and octagonal respectively as presented in Figure 1. The left wall was kept at the constant higher temperature while the right at the constant lower temperature. The other walls are insulated. The heated and cooled walls are of unit side length ( $L=1$ ), but the other dimensions of walls are given in Table 1. The working fluid is  $\text{Al}_2\text{O}_3$ -water nanofluid and the properties are introduced in Table 2.

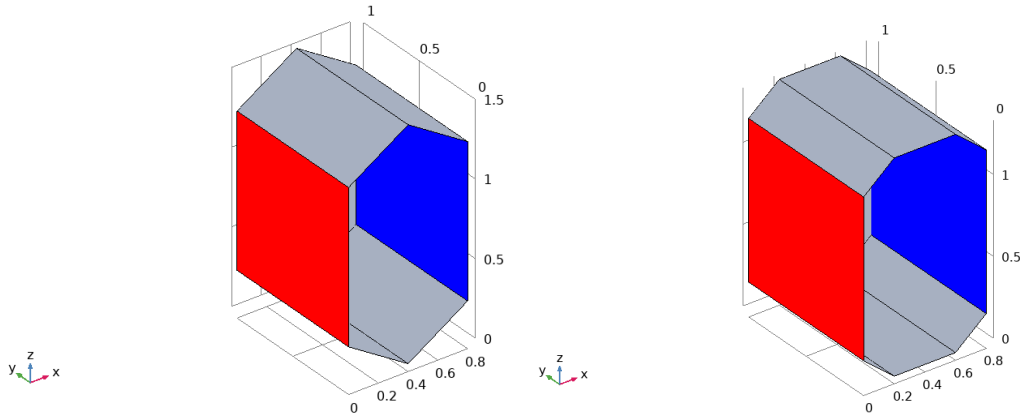
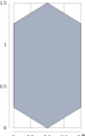



Fig. 1. The cavity configurations

**Table 1**  
 The considered cases details

| Case   | No. of walls | X/L | Y/L | Z/L   | V/L <sup>3</sup> | A <sub>Surface</sub> /L <sup>2</sup> | A <sub>Cold</sub> /L <sup>2</sup> | A <sub>Hot</sub> /L <sup>2</sup> |
|--|--------------|-----|-----|-------|------------------|--------------------------------------|-----------------------------------|----------------------------------|
|   | 8            | 0.8 | 1   | 1.5   | 1                | 5.887                                | 1                                 | 1                                |
|  | 10           | 0.8 | 1   | 1.333 | 1                | 5.841                                | 1                                 | 1                                |

**Table 2**  
 The thermophysical properties [57]

|                                | $\rho$ | $C_p$ | K     | $\beta$   |
|--------------------------------|--------|-------|-------|-----------|
| Pure Water                     | 997.1  | 4179  | 0.613 | 0.0002100 |
| Al <sub>2</sub> O <sub>3</sub> | 3880   | 765   | 40    | 0.0000085 |

### 3. The Governing Equations

Number of assumptions are supposed to describe the governing equations of the flow and heat transfer fields

- i. Steady, incompressible, laminar flow in three dimensions.
- ii. The heat generation and radiation are neglected.
- iii. The water base fluid and the alumina nanoparticles are in thermal equilibrium.
- iv. Steady thermophysical characteristics of the flow corresponding to approximation of Boussinesq.

The assumed governing equations are [52]

(a) The continuity

$$\frac{\partial u}{\partial x} + \frac{\partial v}{\partial y} + \frac{\partial w}{\partial z} = 0 \tag{1}$$

(b) The x component of momentum

$$\rho_{nf} \left( u \frac{\partial u}{\partial x} + v \frac{\partial u}{\partial y} + w \frac{\partial u}{\partial z} \right) = - \frac{\partial P}{\partial x} + \mu_{nf} \left( \frac{\partial^2 u}{\partial x^2} + \frac{\partial^2 u}{\partial y^2} + \frac{\partial^2 u}{\partial z^2} \right) \quad (2)$$

(c) The y component momentum

$$\rho_{nf} \left( u \frac{\partial v}{\partial x} + v \frac{\partial v}{\partial y} + w \frac{\partial v}{\partial z} \right) = - \frac{\partial P}{\partial y} + \mu_{nf} \left( \frac{\partial^2 v}{\partial x^2} + \frac{\partial^2 v}{\partial y^2} + \frac{\partial^2 v}{\partial z^2} \right) - \rho_{nf} g \quad (3)$$

(d) The z component momentum

$$\rho_{nf} \left( u \frac{\partial w}{\partial x} + v \frac{\partial w}{\partial y} + w \frac{\partial w}{\partial z} \right) = - \frac{\partial P}{\partial z} + \mu_{nf} \left( \frac{\partial^2 w}{\partial x^2} + \frac{\partial^2 w}{\partial y^2} + \frac{\partial^2 w}{\partial z^2} \right) \quad (4)$$

(e) The energy

$$u \frac{\partial T}{\partial x} + v \frac{\partial T}{\partial y} + w \frac{\partial T}{\partial z} = \alpha_{nf} \left( \frac{\partial^2 T}{\partial x^2} + \frac{\partial^2 T}{\partial y^2} + \frac{\partial^2 T}{\partial z^2} \right) \quad (5)$$

The nanofluid properties [58,59]

$$\alpha_{nf} = \frac{K_{nf}}{(\rho c_p)_{nf}} \quad (6)$$

$$\mu_{nf} = \frac{\mu_f}{(1-\phi)^{2.5}} \quad (7)$$

$$\rho_{nf} = (1 - \phi)\rho_f + \phi\rho_p \quad (8)$$

$$(\rho c_p)_{nf} = (1 - \phi)(\rho c_p)_f + \phi(\rho c_p)_p \quad (9)$$

The thermal conductivity of nanofluid is described by Maxwell Garnetts model for spherical nanoparticles

$$\frac{K_{nf}}{K_f} = \frac{(K_p + 2K_f) - 2\phi(K_f - K_p)}{(K_p + 2K_f) + \phi(K_f - K_p)} \quad (10)$$

The FEM technique is employed to solve these equations numerically. The system of equations is converted to the dimensionless formula which controlling the number of variables by defining the following parameters

$$X, Y, Z = \frac{(x,y,z)}{L} \quad (11)$$

$$U, V, W = \frac{(u,v,w)}{\alpha_{bf}/L} \quad (12)$$

$$P = \frac{p + \rho_{bf} g y}{(\rho_{nf} \alpha_{bf}^2 / L)} \quad (13)$$

$$\theta = \frac{T_h - T}{\Delta T} \quad (14)$$

$$\Delta T = T_h - T_c \quad (15)$$

Therefore, the governing equations in dimensionless form becomes as

$$\frac{\partial U}{\partial X} + \frac{\partial U}{\partial Y} + \frac{\partial U}{\partial Z} = 0 \quad (16)$$

$$U \frac{\partial U}{\partial X} + V \frac{\partial U}{\partial Y} + W \frac{\partial U}{\partial Z} = -\frac{\partial P}{\partial X} + \frac{\mu_{nf}}{\alpha_f \rho_{nf}} \left( \frac{\partial^2 U}{\partial X^2} + \frac{\partial^2 U}{\partial Y^2} + \frac{\partial^2 U}{\partial Z^2} \right) \quad (17)$$

$$U \frac{\partial V}{\partial X} + V \frac{\partial V}{\partial Y} + W \frac{\partial V}{\partial Z} = -\frac{\partial P}{\partial Y} + \frac{\mu_{nf}}{\alpha_f \rho_{nf}} \left( \frac{\partial^2 V}{\partial X^2} + \frac{\partial^2 V}{\partial Y^2} + \frac{\partial^2 V}{\partial Z^2} \right) \quad (18)$$

$$U \frac{\partial W}{\partial X} + V \frac{\partial W}{\partial Y} + W \frac{\partial W}{\partial Z} = -\frac{\partial P}{\partial Z} + Ra \times Pr \times \theta \times \frac{\rho_f \beta_{nf} \mu_{nf}}{\rho_{nf} \beta_f \alpha_f \rho_{nf}} \left( \frac{\partial^2 W}{\partial X^2} + \frac{\partial^2 W}{\partial Y^2} + \frac{\partial^2 W}{\partial Z^2} \right) \quad (19)$$

$$U \frac{\partial \theta}{\partial X} + V \frac{\partial \theta}{\partial Y} + W \frac{\partial \theta}{\partial Z} = \frac{\alpha_{nf}}{\alpha_f} \left( \frac{\partial^2 \theta}{\partial X^2} + \frac{\partial^2 \theta}{\partial Y^2} + \frac{\partial^2 \theta}{\partial Z^2} \right) \quad (20)$$

These equations are solved with the supposed initial and boundary conditions that are presented in Figure 1. The initial temperature of the fluid domain is ( $T_i$ ) which given by

$$T_i = (T_h + T_c)/2 \quad (21)$$

The suggested boundary conditions are

$$(i) \quad \text{No slip is considered for all walls: } U=V=W=0 \quad (22)$$

$$(ii) \quad \text{The hot temperature is supplied on the left vertical sidewall: } X=0, \theta=1 \quad (23)$$

$$(iii) \quad \text{The cold temperature is supplied on the right vertical sidewall: } X=1, \theta=0 \quad (24)$$

$$(iv) \quad \text{Other walls are insulated: } \frac{\partial \theta}{\partial X} = \frac{\partial \theta}{\partial Y} = \frac{\partial \theta}{\partial Z} = 0 \quad (25)$$

#### 4. Numerical Methodology

The laminar steady flow of nanofluid and the free convection heat transfer accompanied with it inside the described enclosures are solved by employing the finite element numerical method (FEM). The grid independency is examined in accordance to the average (Nu) value stability. The test procedure is introduced in Table 3 for the hexagonal cavity. The selected meshes for the two cavities are as shown in Figure 2 and Table 4. The suitable mesh is guided by two roles; the time consumed and the percentage error. A good sign on the validation of the current results is the satisfied previous studies as presented in Table 5. For more accuracy, the present contours of stream lines and isotherm lines are validated in Figure 3.

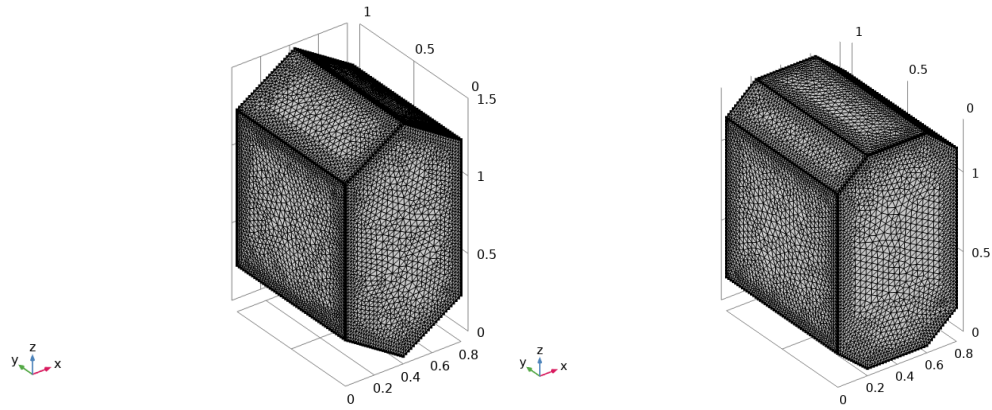


**Fig. 2.** The selected mesh



**Table 3**

The grid independence at  $Ra=10^4$  and  $\varphi = 0.05$  for the hexagonal cavity

| Total elements | Boundary elements | Edge elements | Nu     | The consumed time (sec) |
|----------------|-------------------|---------------|--------|-------------------------|
| 78133          | 4044              | 234           | 2.3110 | 14                      |
| 158709         | 6316              | 290           | 2.5742 | 22                      |
| 178643         | 10712             | 430           | 2.9063 | 31                      |
| 243279         | 17038             | 674           | 2.9988 | 64                      |
| 556201         | 24430             | 674           | 2.9989 | 171                     |

**Table 4**

The selected grid for the present cases

| Cases   | Total elements | Boundary elements | Edge elements |
|---|----------------|-------------------|---------------|
|  | 243279         | 17038             | 674           |
|  | 260742         | 17852             | 772           |

**Table 5**

The average Nu validation with other data

| Author                            | $Ra = 10^4$ | $Ra = 10^5$ |
|-----------------------------------|-------------|-------------|
| Tric <i>et al.</i> , [60]         | 2.050       | 4.34        |
| Peng <i>et al.</i> , [61]         | 2.080       | 4.38        |
| Purusothaman <i>et al.</i> , [62] | 2.059       | 4.35        |
| Present                           | 2.045       | 4.37        |

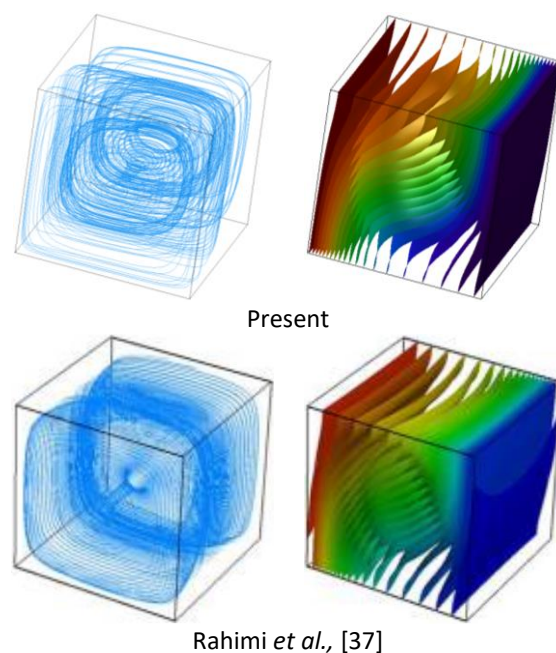


**Fig. 3.** Validation of the streamlines (left) and isotherm lines (right) with Rahimi *et al.*, [37]

## 5. Results

The results are divided into four main categories; the fluid flow, the pressure field, the heat transfer field and the Nusselt number. The criteria of the different parameters effects on these fields are discovered in the following sections.

### 5.1 The Fluid Flow Field

The streamlines of the two cavities at ( $\phi=0.05$ ) and ( $Ra=10^4$  and  $10^5$ ) are presented in Figure 4 in three-dimensional. The fluid flows in clockwise circulation from the hot wall towards the cold wall. Where the physical convection process causing the movement of the hot fluid that adjoining to the hot wall up and the cold fluid that adjoining the cold wall down. The collide of the hot fluid by the upper wall causing decelerating of the vertical upward velocity and flows horizontally towards the cold wall. On the other hand, the cold fluid meets the base wall and decelerating the downward vertical velocity and accelerating the horizontal velocity towards the hot wall. This circulation is repeated many times causing the mentioned fluid flow configuration. For more investigation of the fluid flow, three longitudinal sections at ( $Y=0.25, 0.5, 0.75$ ) to present the streamlines at ( $\phi=0.05$  and  $Ra=10^4$ ) as shown in Figure 5. The three planes introduce a similar configuration but the central plane ( $Y=0.5$ ) has the denser lines. While the terminal planes ( $Y=0.25, 0.75$ ) have the same count of lines, that means the flow is identical around the central plane. The more density of lines in central plane can be explained as the faraway from the cavity walls which work as a flow deceleration and their effect become weak at the central location unsimilar to the other two planes. The central plane will be depended on to present all the fluid flow parameters in the coming sections. The Figure 6 represent the streamlines for the two cavities at different solid volume fraction (a)  $\phi=0.01$  and (b)  $\phi=0.05$ . For the two cavities the configuration of the stream lines is circulated clockwise with center core have elliptical shape at ( $Ra=10^3$ ) with the longer axis is parallel to the vertical hot and cold walls. This elliptical core tends to inclined a little towards the cold wall at ( $Ra=10^4$ ). At ( $Ra=10^5$ ) the ellipse elongates horizontally where its shape converts to rectangle with the left corner higher than the right

corner position by means twisted slightly towards the left hot wall. This rectangle increased in width till the bounded streamlines are being closer to each other near the hot and cold walls at ( $Ra=10^6$ ). The core region fluid is in stagnant state. The same configurations are observed for the solid volume fraction of ( $\phi=0.05$ ) except that the stagnant regions are less than the case of ( $\phi=0.01$ ) in a little rate for all the  $Ra$  range. This behavior can be explained as that the mass increase results in higher continuity in flow.

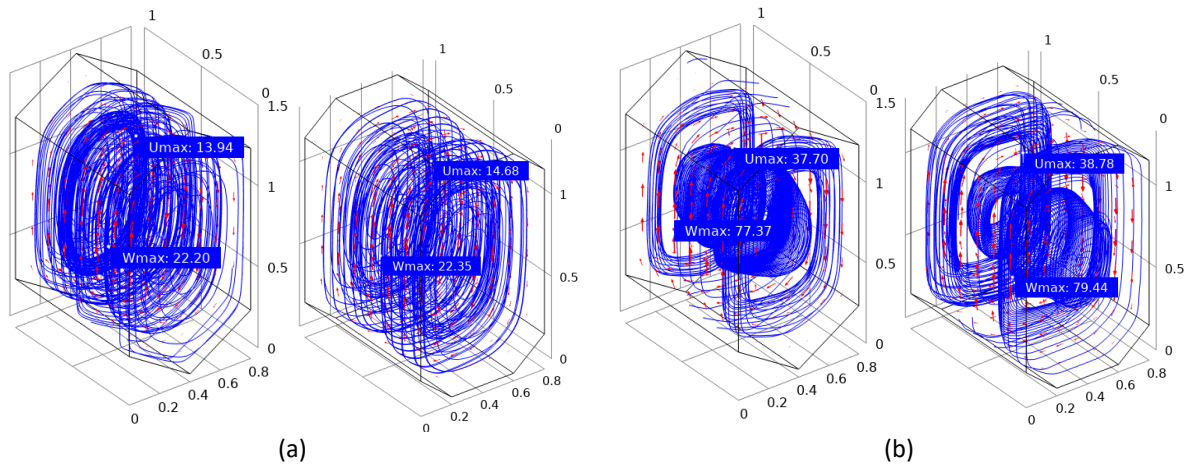


**Fig. 4.** The streamlines for the two cases at  $\phi = 0.05$ ; (a)  $Ra= 10^4$ , (b)  $Ra = 10^5$

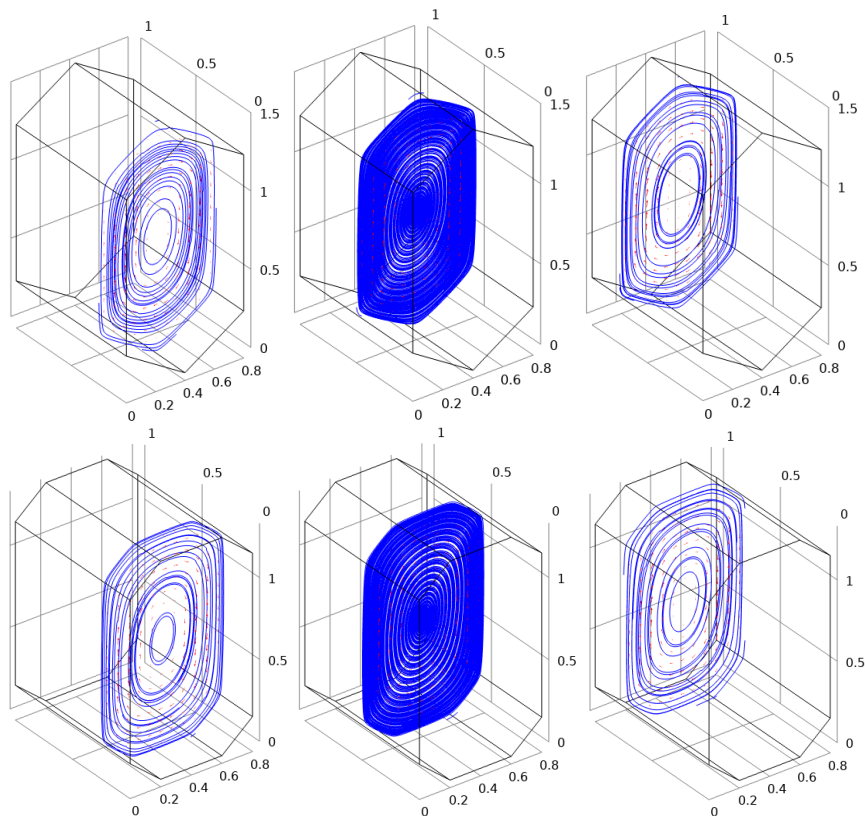


**Fig. 5.** The streamlines for the two cases at  $\phi = 0.05$  and  $Ra = 10^4$  on planes ( $Y = 0.25, 0.5, 0.75$ ) (left to right)



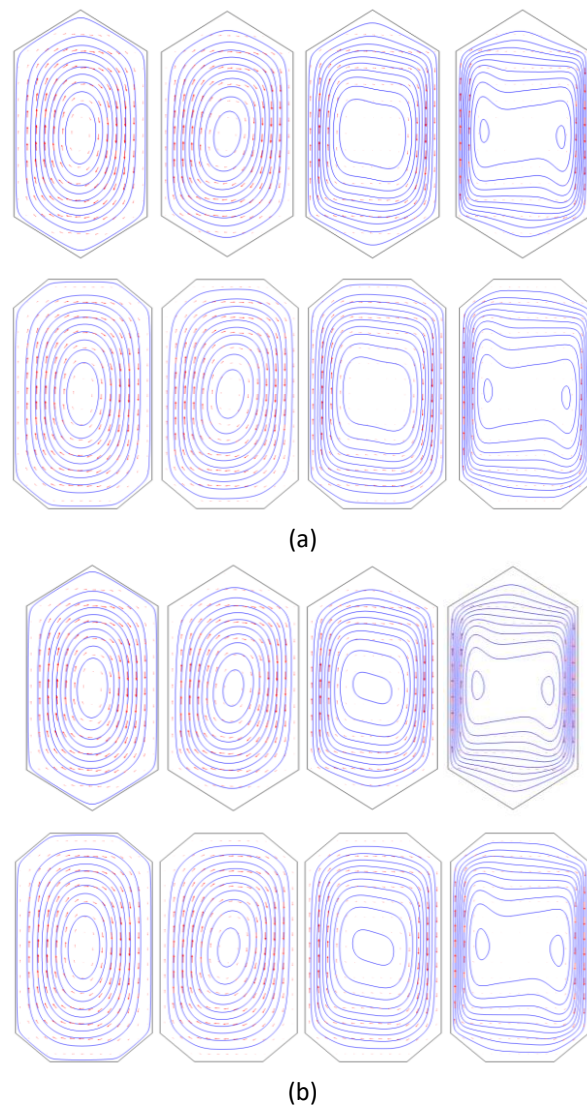


**Fig. 6.** The streamlines on plane ( $Y=0.5$ ) at  $10^3 \leq Ra \leq 10^6$  (left to right); (a)  $\phi = 0.01$ , (b)  $\phi = 0.05$

The horizontal velocity ( $U$ ) of the two cavities is presented on the central plane in Figure 7 for two values of the nano particles solid volume fractions. Noticing that for the different volume fractions the velocity profile is similar for each cavity shape. The horizontal velocity ( $U$ ) turns in two circulated vortices between the upper and base walls of the cavities one above the other. Where these vortices taking the shape of the base and tip of each cavity at the locations adjacent to these walls. These circulations are clockwise at the upper half of the cavity and counter clockwise at the lower part of the cavity as shown in Figure 8 where the negative velocities mean the same value but in the reverse direction. The circulations have single circular core at ( $Ra= 10^3$  and  $10^4$ ) and double circular cores at the corners of the cavities at ( $Ra= 10^5$  and  $10^6$ ). The horizontal velocity ( $U$ ) for the two cavities accelerated with the solid volume fraction increase. On the other hand, this velocity nearly the same for the two cavities for ( $Ra=10^3, 10^4, 10^5$ ) but the difference appears clearly at ( $Ra=10^6$ ). For the hexagonal, the increase ( $\Delta U=1.002\%$ ) and for octagonal nearly ( $\Delta U=0.8\%$ ) for ( $\Delta\phi=0.04$  at  $Ra=10^6$ ). The hexagonal cavity has higher horizontal velocity ( $U$ ) than the octagonal cavity for the same flow conditions; by means the solid volume fraction and  $Ra$ . This phenomenon is due to the shape of the tip and base of the two cavities. Where for the hexagonal one, the height of the triangular shape of the tip is giving the space to the velocity to propagate highly while the less height of the first corner

of the octagonal tip and the subsequent straight part are contribute in the velocity deceleration. It is also observed that the maximum velocity (U) is located inside the centers of cores for the two cavities.

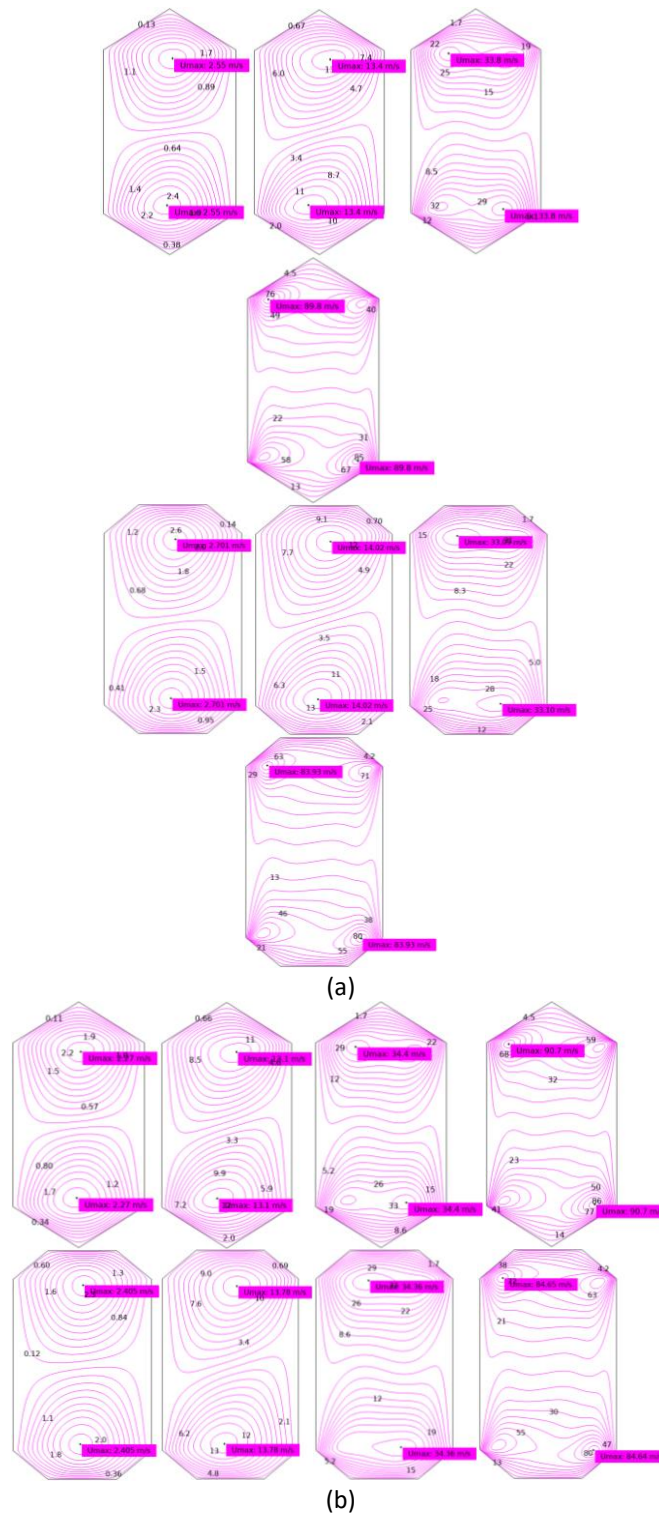


**Fig. 7.** The horizontal velocity U (m/s) contour on plane (Y=0.5) at  $10^3 \leq Ra \leq 10^6$  (left to right); (a)  $\phi = 0.01$ , (b)  $\phi = 0.05$

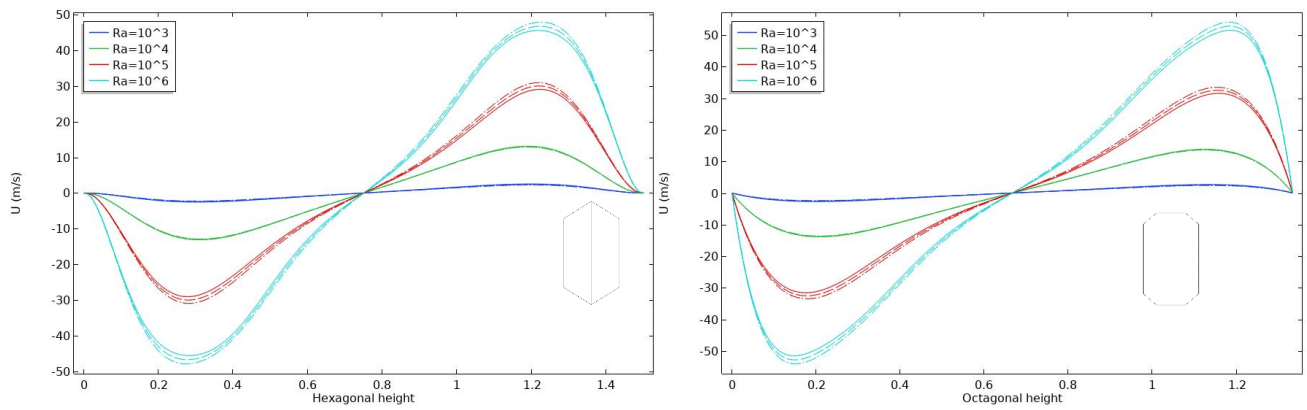


**Fig. 8.** The horizontal velocity  $U$  along the central height

The vertical velocity ( $W$ ) turns in two circulated vortices between the left and right walls of the cavities one beside the other as it presented in Figure 9. Also, these vortices have single core but of elliptical shape with its longer axis parallel to the cavity height for all the  $Ra$  range.

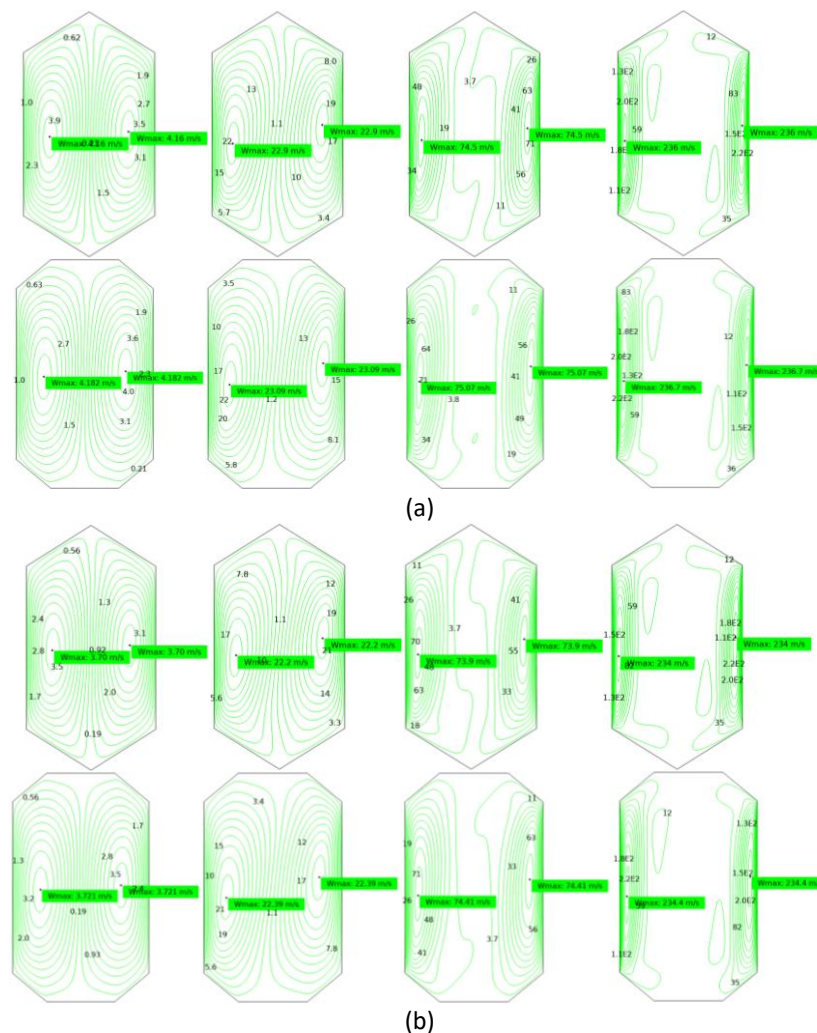


**Fig. 9.** The vertical velocity  $W$  (m/s) contour on plane ( $Y=0.5$ ) at  $10^3 \leq Ra \leq 10^6$  (left to right); (a)  $\phi = 0.01$ , (b)  $\phi = 0.05$

The circulations are clockwise at the right half of the cavity which close to the hot wall and counter clockwise at the left part of the cavity which close to the cold wall as shown in Figure 10. The negative velocities mean the same value but in the reverse direction as like as (U). These cores are touch each other at the center of the cavity for ( $Ra=10^3$  and  $10^4$ ). While it began to be far apart from each other for ( $Ra=10^5$  and  $10^6$ ) for the two cavities and all solid volume fraction values. Unlike the horizontal velocity (U), the vertical velocity (W) is decelerating with the solid volume fraction increase. And the hexagonal cavity has lower vertical velocity than the octagonal cavity by a very little rate for the same flow parameters. For the hexagonal, the decrees ( $\Delta W=0.15\%$ ) and for octagonal nearly ( $\Delta W=0.02\%$ ) for ( $\Delta\phi=0.04$  at  $Ra=10^6$ ). The maximum velocity is located inside the centers of cores for the two cavities also. Another important observation is presented in Figure 11 and Figure 12, which is the relation between the horizontal (U) and vertical (W) velocities and their behavior towards Ra variation. Both velocities are augmented by Ra increase and always for all solid volume fractions and in the two cavities the horizontal velocity (U) is lower than the vertical one (W). But, the important observation of the cavity configuration on the solid volume fraction effect on the flow. Where the variation in the velocities (U) and (W) inside the hexagonal are higher than that inside the octagonal.

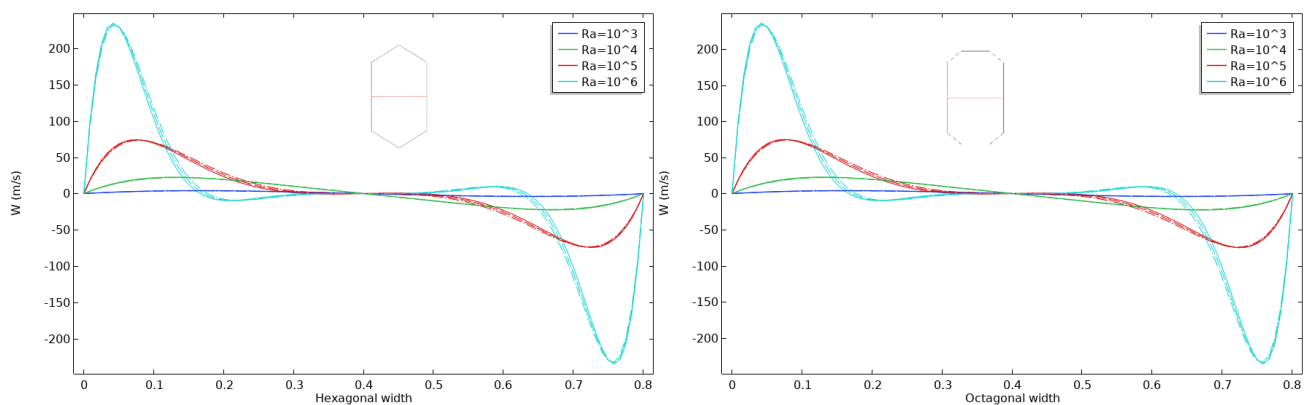


**Fig. 10.** The vertical velocity W along the central width

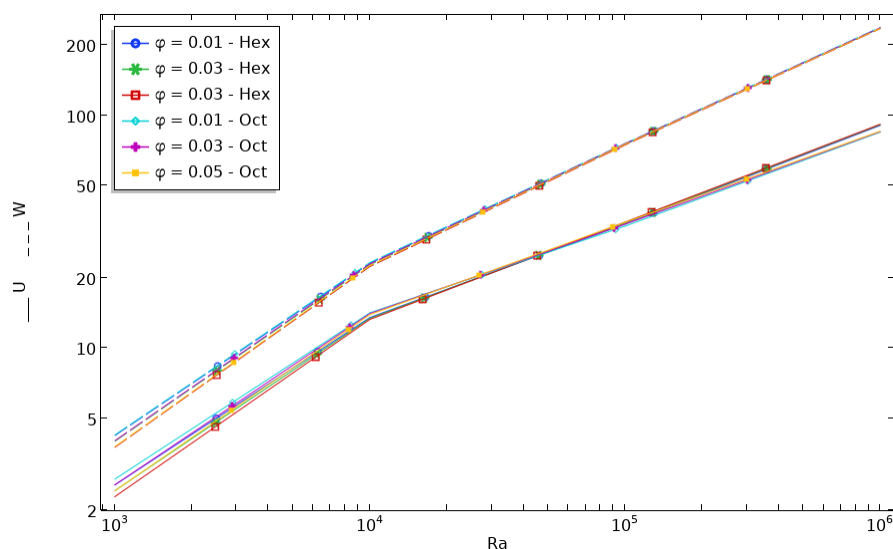


**Fig. 11.** The maximum horizontal U and vertical W velocities versus Ra

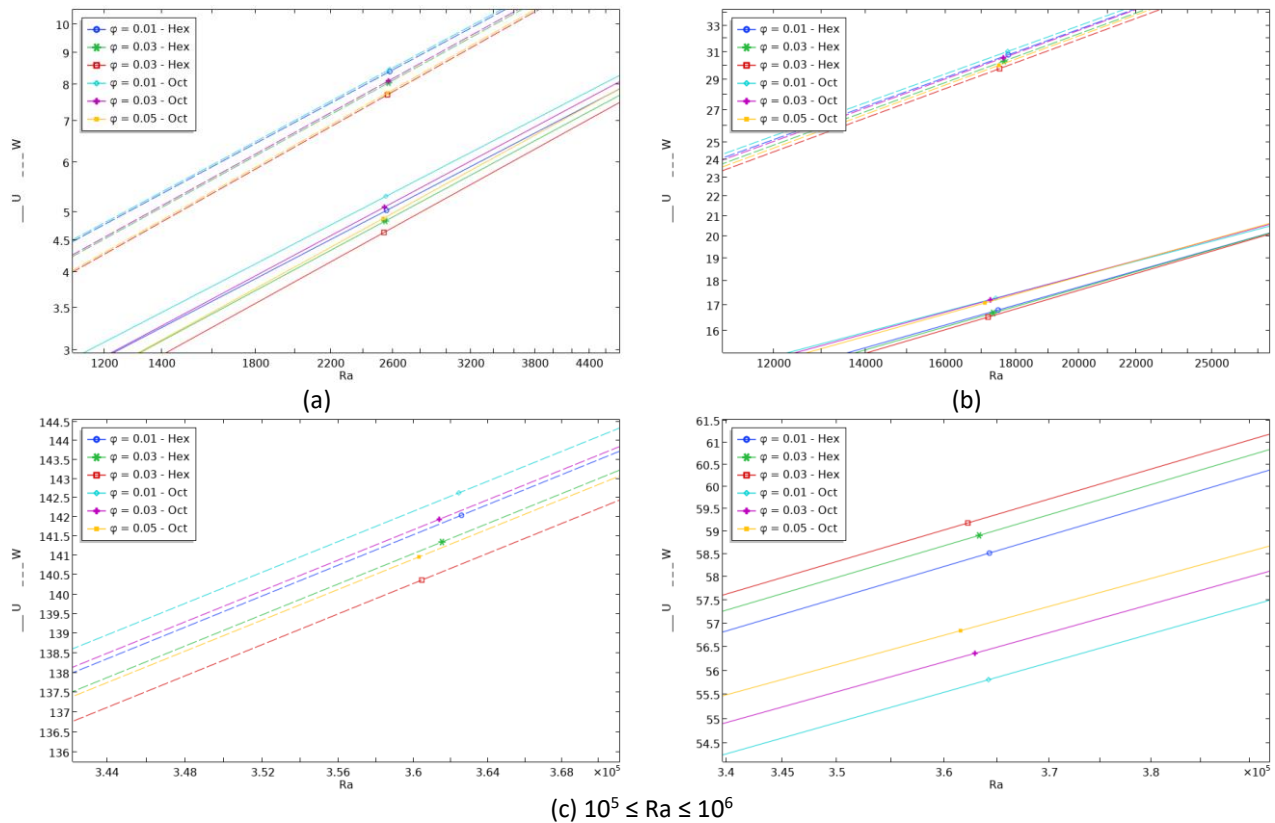


**Fig. 12.** The maximum horizontal U and vertical W velocities versus different Ra ranges; (a)  $10^3 \leq Ra \leq 10^4$ , (b)  $10^4 \leq Ra \leq 10^5$

## 5.2 The Pressures Field

The total pressure is the continuous physical force exerted against the cavity walls in contact with the fluid. The total pressure is consisting of two parts of pressure where their collect given constant value everywhere inside the enclosed domain according to Bernoulli principle in the incompressible flow conditions. The static pressure which is the amount of pressure exerted by the stationary fluid. While the dynamic pressure or the velocity pressure is the pressure exerted by the fluid movement. For the two cavities the maximum static pressure located at the deeper central point of the cavity which located below the core of the flow vortices that nearly in stable state and the longer column of fluid above it as shown in Figure 13 and Figure 14 which present the constant static pressure lines and the static pressure along the central width and height of the two cavities respectively. Also, the static pressure nearly constant along the same depth points as it represented by the constant pressure lines along the cavity's width. The same behavior is observed for all the solid volume fractions and Ra. The static pressure for the two cavities is directly proportional to the Ra but inversely to the solid volume fraction. But the static pressure of the hexagonal cavity is more than the octagonal for the same working conditions due to the longer height of the hexagonal cavity. On the other hand, the dynamic pressure profile is similar to the streamlines profile and the maximum value is at the same location of the maximum vertical velocity (W) as shown in Figure 15.

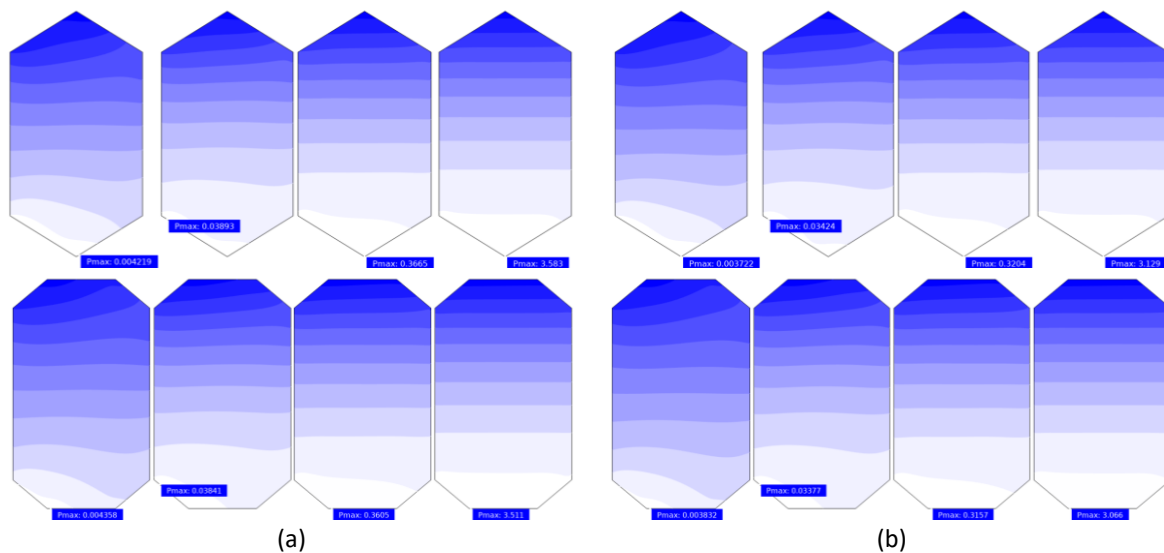


**Fig. 13.** The isobaric lines contour of the static pressure (Mpa) on the plane ( $Y=0.5$ ) for  $10^3 \leq Ra \leq 10^6$  (left to right); (a)  $\phi = 0.01$ , (b)  $\phi = 0.05$

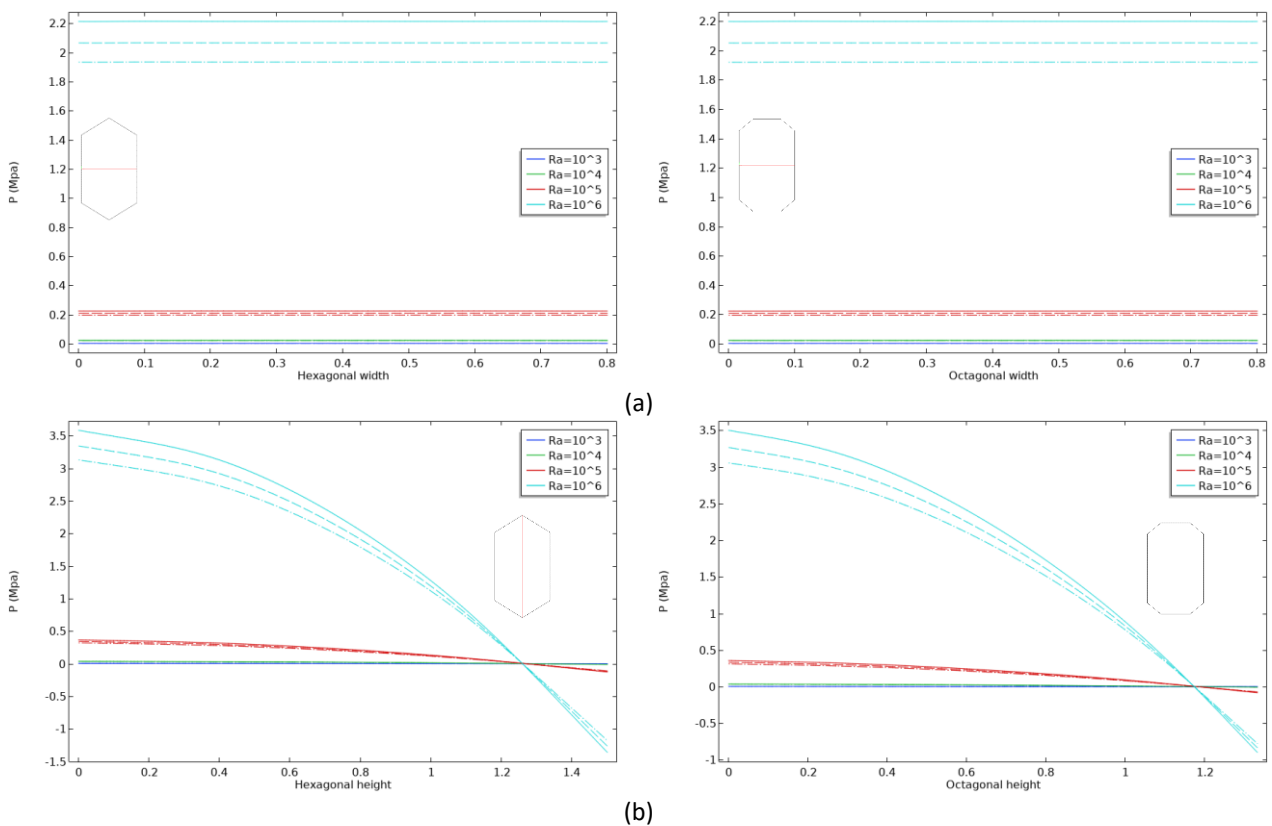


**Fig. 14.** The static pressure versus Ra: continous line ( $\phi=0.01$ ), dashed line ( $\phi=0.03$ ), dashed dotted line ( $\phi=0.05$ ); (a) Along the cavity width (X-axis), (b) Along the cavity height (Z-axis)

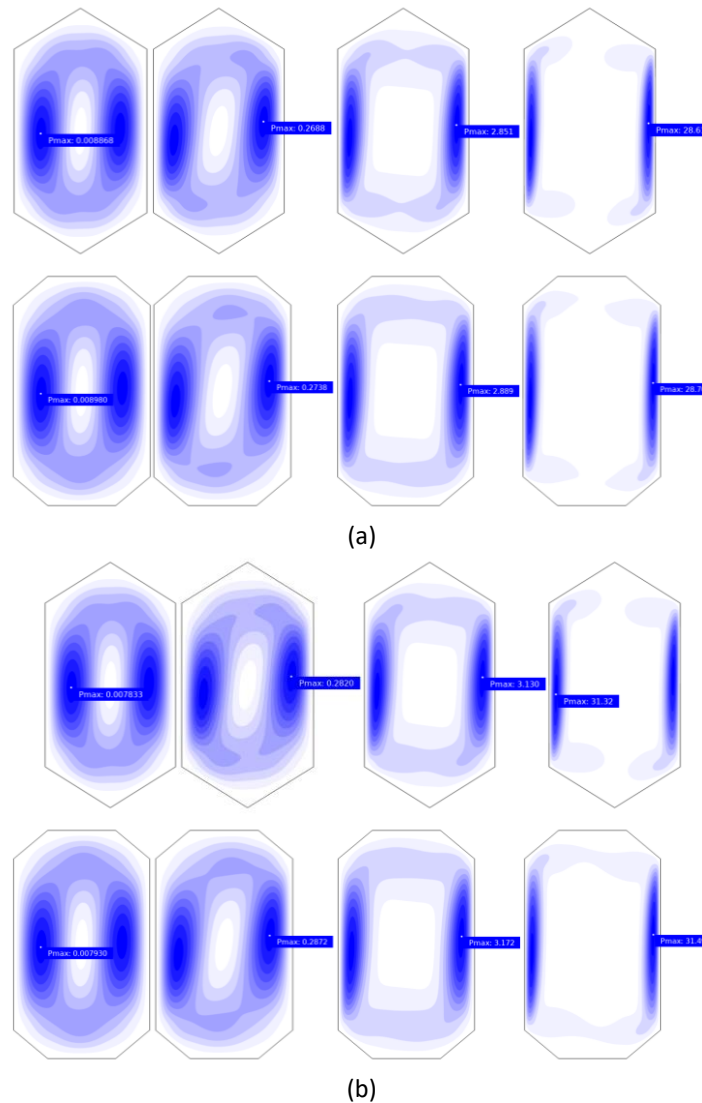


**Fig. 15.** The isobaric lines contour of the dynamic pressure (Mpa) on the plane ( $Y=0.5$ ) for  $10^3 \leq Ra \leq 10^6$  (left to right); (a)  $\phi = 0.01$ , (b)  $\phi = 0.05$

As like the static pressure, the dynamic pressure proportional directly with  $Ra$ , but unlike it, also proportional directly with the solid volume fraction as shown in Figure 16. Because that the dynamic pressure proportion directly to the density which in turn increases with the solid volume fraction increase. But the dynamic pressure of the hexagonal cavity is less than the octagonal for the same working conditions. This phenomenon can be explained as that the flow is controlled more by the vertical velocity ( $W$ ) which for the hexagonal cavity is less than it for the octagonal cavity. which lead to the same behavior by the dynamic pressure.

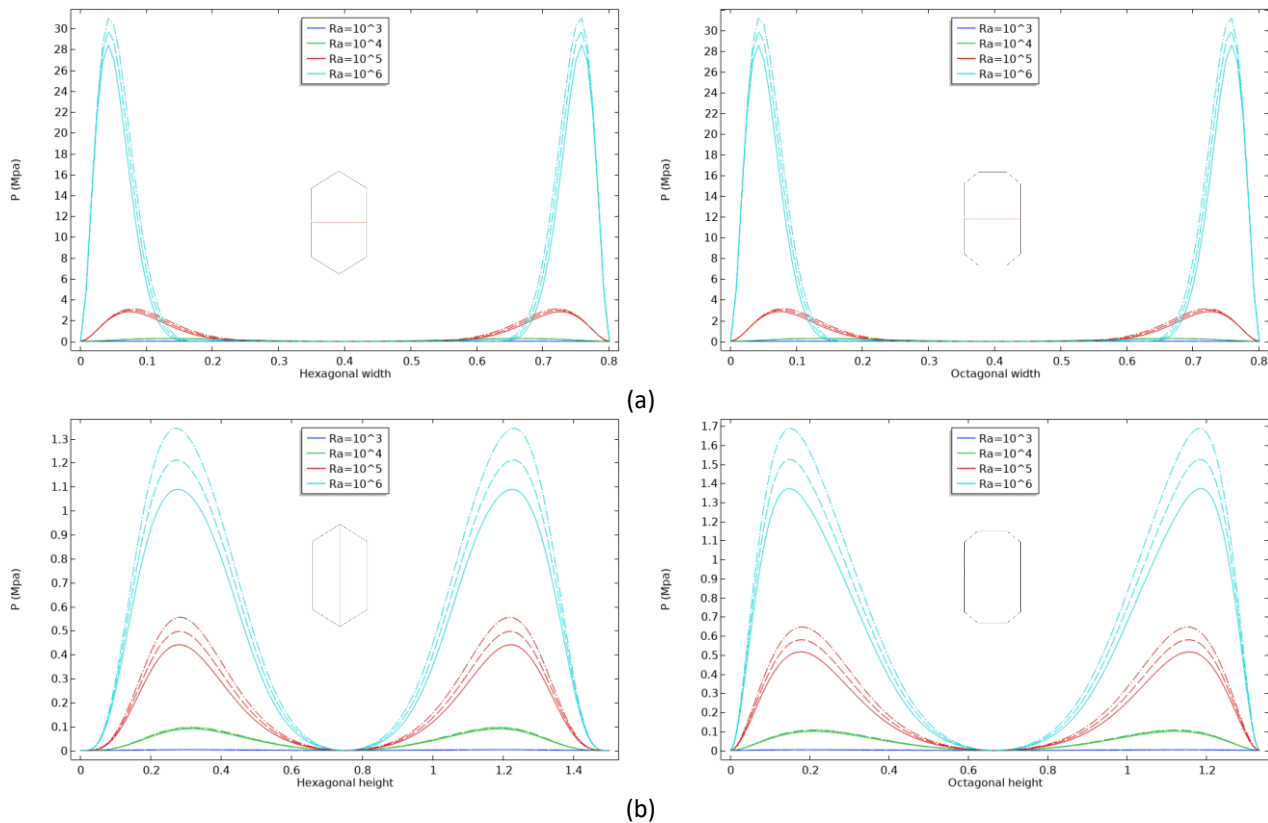


**Fig. 16.** The dynamic pressure versus Ra: continuous line ( $\phi=0.01$ ), dashed line ( $\phi=0.03$ ), dashed dotted line ( $\phi=0.05$ ); (a) Along the cavity width (X-axis), (b) Along the cavity height (Z-axis)

### 5.3 The Thermal Field

The constant temperature lines or the isotherm lines contour for the two cavities are presented in Figure 17 at ( $\phi=0.05$ ) with ( $Ra=10^4$  and  $10^5$ ). And the contours on the three selected planes ( $Y=0.25, 0.5, 0.75$ ) at ( $\phi=0.05$ ) and ( $Ra=10^4$ ) are viewed in Figure 18. Unlike the stream lines, there is no clear difference among the three profile planes. Although, the central plane at ( $Y=0.5$ ) still the preferred plane to present the heat transfer data. Figure 19 introduces the isotherm lines of the two cavities for different solid volume fractions versus Ra. The part (a) of this figure is at ( $\phi=0.01$ ), for the two cavities the isotherm lines nearly stay straight (tilted towards the right slightly) and parallel to the vertical walls of the cavities at ( $Ra=10^3$  and  $10^4$ ). Then, the nonlinearity of these lines is appearing obviously to announce the convection control on the heat transfer field completely at ( $Ra=10^5$  and  $10^6$ ). The heat convection is explained previously in section (5.1). Where the physical convection process causing the movement of the hot fluid up and the cold fluid down causing the presented heat flow configuration. The Figure 19(b), preview the cavities at ( $\phi=0.05$ ) and different Ra. It is clear that the behavior of the isotherm lines is identical to that in Figure 19(a). But, the Figure 20 and Figure 21, proving that for the same point in the flow, the temperature is higher for the higher solid volume fraction and lower Ra for the two cavities at the left half of the cavity. Revers behavior appears at the other half.

Another important observation can be concluded from the Figure 21 which describes the temperature drop along the cavity width. For ( $Ra=10^3$ ) the drop is linear, while the behavior of the cases with ( $Ra=10^4$  and  $10^5$ ) are similar which are nearly quadratically which concave up at the first half and concave down at the second half of the cavity. The inverse of the concave orientation occurs at the mid distance between the hot and cold walls. For ( $Ra=10^6$ ), the quadratically regions are



confine at the location of (1/8) from the hot wall concave up and from (7/8) to the cold wall concave down while the distance in between is nearly still constant or no drop in temperature appears. The temperature profile for the two cavities is similar but the octagonal cavity takes longer time to reach the same results of the hexagonal cavity. The increase in the time consumed is about ( $\Delta t=4.65\%$ ) which can be caused due to the more complexity in the octagonal geometry.

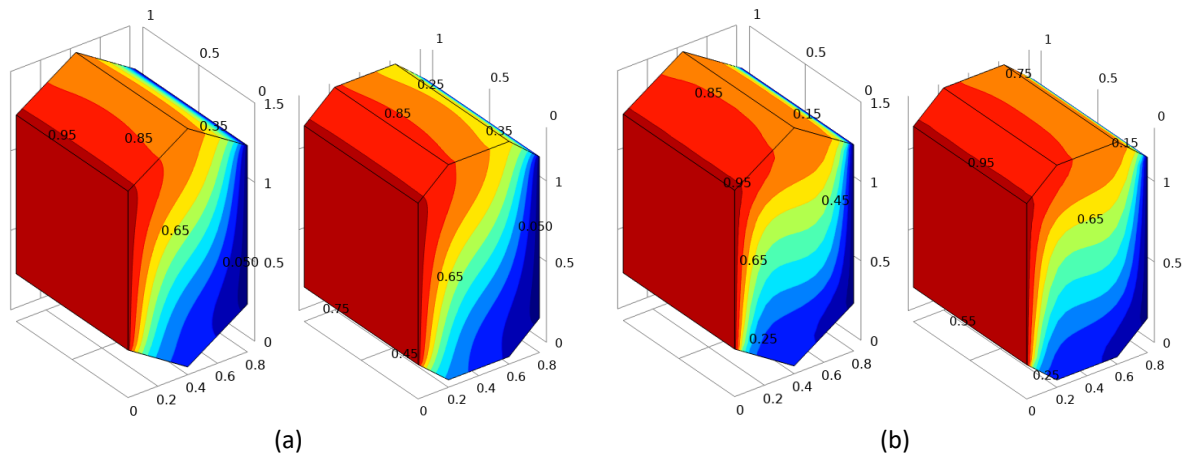


**Fig. 17.** The isotherm surfaces for the two cases at  $\phi = 0.05$ ; (a)  $Ra = 10^4$ , (b)  $Ra = 10^5$

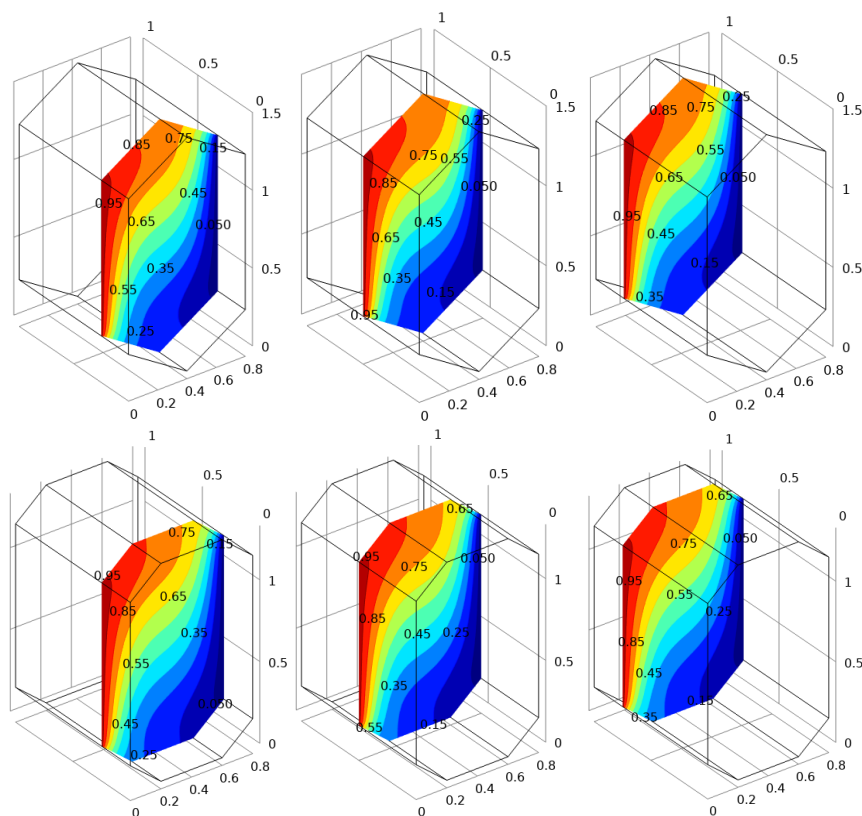


**Fig. 18.** The isotherm lines for the two cases at  $\phi = 0.05$  and  $Ra = 10^4$  on planes ( $Y = 0.25, 0.5, 0.75$ ) (left to right)

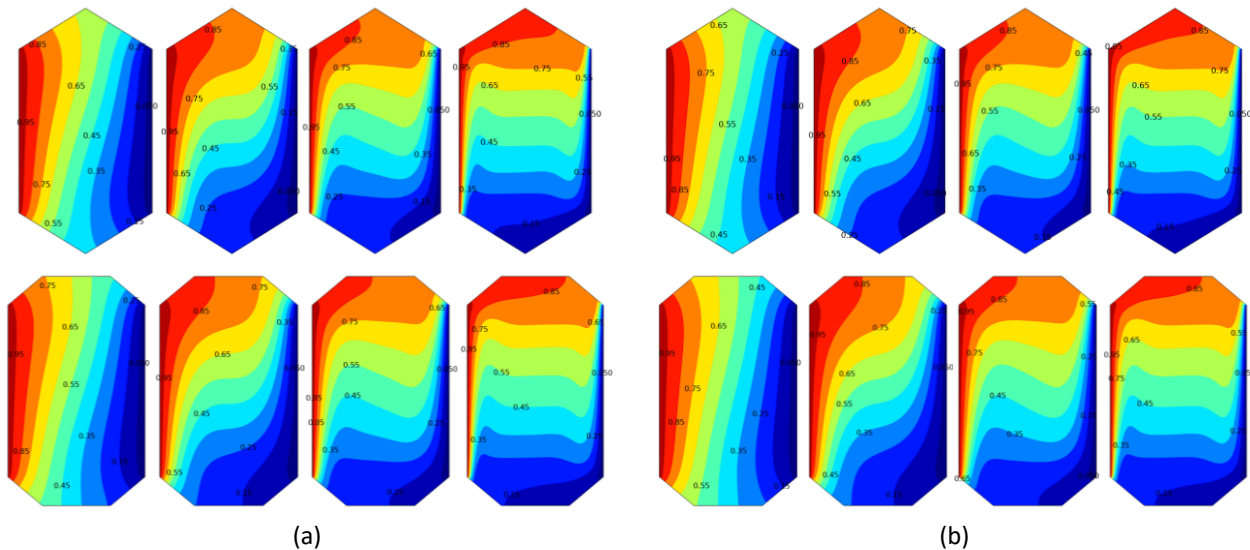


**Fig. 19.** The isothermal lines on plane ( $Y=0.5$ ) at  $10^3 \leq Ra \leq 10^6$  (left to right); (a)  $\phi = 0.01$ , (b)  $\phi = 0.05$

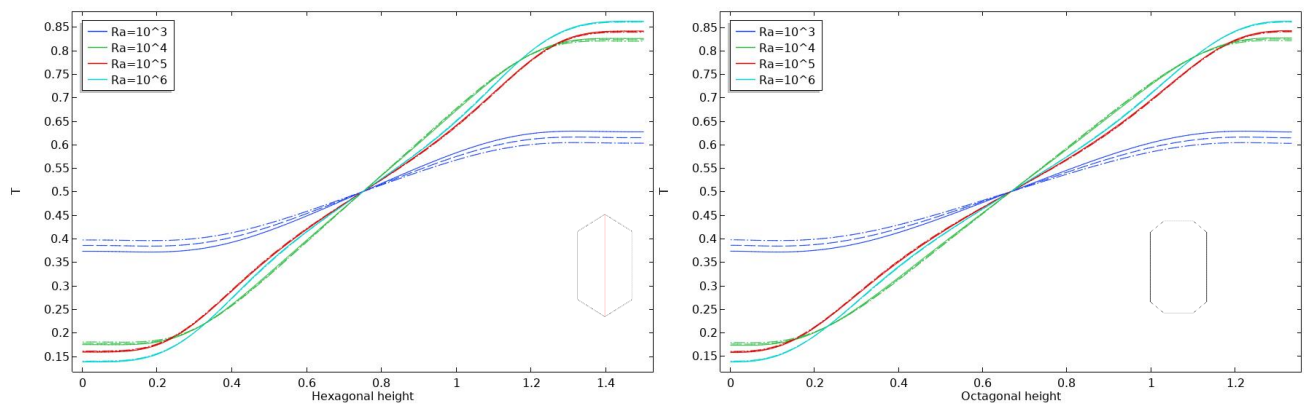


**Fig. 20.** The temperature versus  $Ra$  along the cavity height, continuous line ( $\phi=0.01$ ), dashed line ( $\phi=0.03$ ), dashed dotted line ( $\phi=0.05$ )

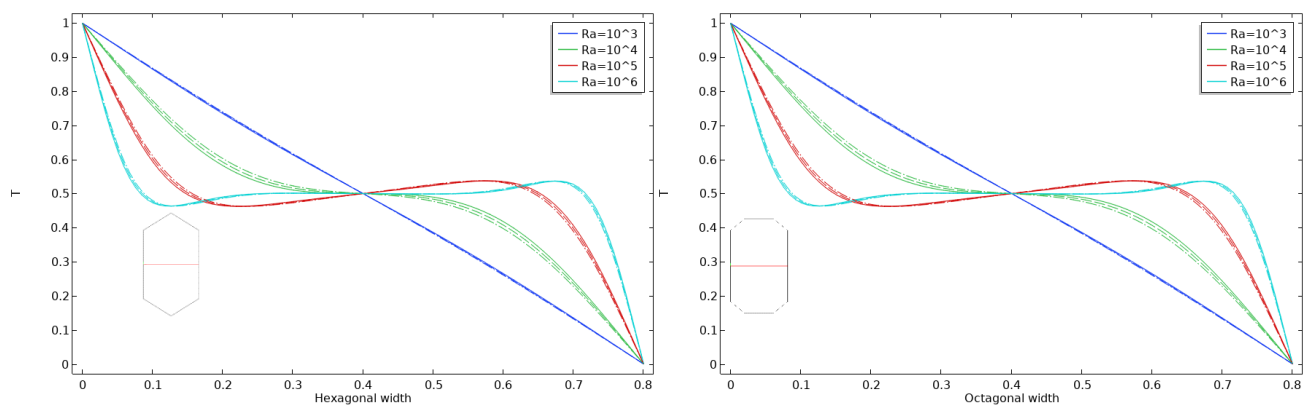


**Fig. 21.** The temperature versus  $Ra$  along the cavity width, continuous line ( $\phi=0.01$ ), dashed line ( $\phi=0.03$ ), dashed dotted line ( $\phi=0.05$ )

#### 5.4 The Nusselt Number

The dimensionless parameter that is measuring the ratio of convection to conduction heat transfer at the boundary layer region. The local  $Nu$  along the hot wall can be defined as [37]

$$Nu_{local} = \frac{h}{k/L} |Hot\ wall| \tag{26}$$

The averaged Nu on the whole hot sidewall is presented as [37]

$$Nu = \int_0^1 \int_0^1 (Nu_{local}) dy dz \tag{27}$$

Figure 22 presents the average (Nu) along the hot wall versus Ra for the two cavities at different solid volume fractions. While Figure 23 shows a maximize view of the same figure for the range ( $10^4 \leq Ra \leq 10^5$ ). Noticing that the average Nu for the two cavities is increases with Ra and solid volume fraction increase. For all flow conditions the average Nu for the octagonal cavity is higher than the hexagonal cavity although the hot wall has the same configuration and dimensions. The Nu increase of the octagonal cavity over the hexagonal cavity for all solid volume fractions is constant which is about ( $\Delta Nu = 0.6\%$ ,  $0.8\%$ ,  $0.7\%$ ,  $0.3\%$ ) for ( $Ra = 10^3$ ,  $10^4$ ,  $10^5$ ,  $10^6$ ) respectively. The maximum enhancement of Nu occurs at ( $Ra=10^4$  and  $10^5$ ) but its minimum enhancement is at ( $Ra=10^6$ ) where the flow tends to be turbulent after this Ra. Indicating that for cavities of the same volume but the overall surface area increase by means of more walls has a positive effect on the heat transfer augmentation. The distribution of the local Nu along the central height of the hot wall of the two cavities is presented in Figure 24. At each Ra, the local Nu drop from its maximum value at the base of the wall and reaching its minimum value at the tip of it. This graduation of the local Nu is nearly unfounded for ( $Ra=10^3$ ) while it is very high at ( $Ra=10^6$ ).

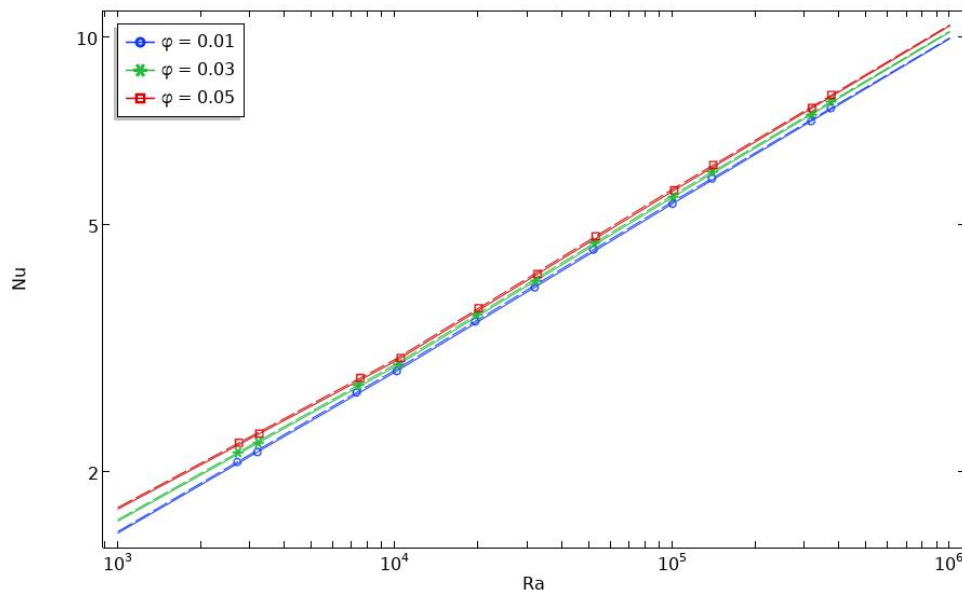


**Fig. 22.** The Nu versus Ra along the left vertical hot wall: continuous line (hexagonal cavity), dashed (octagonal cavity)

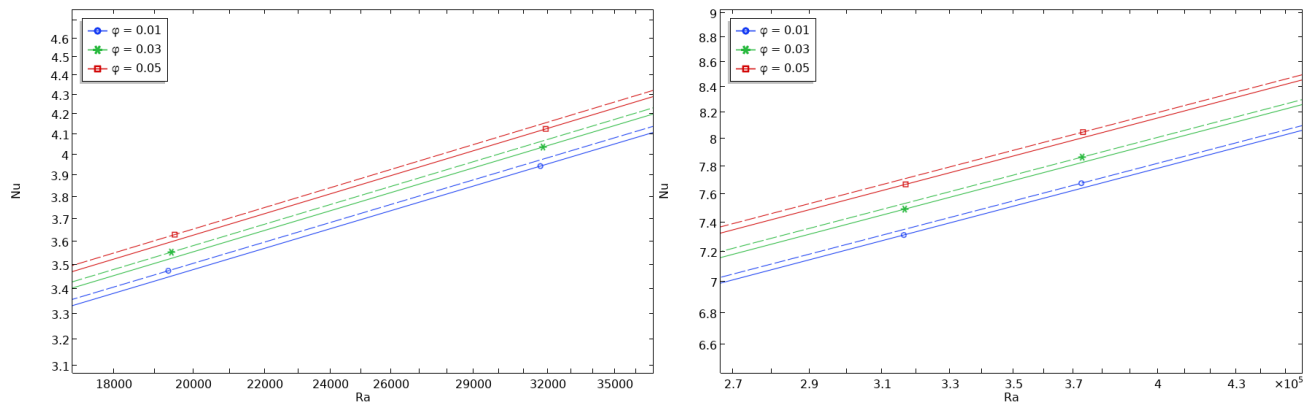


**Fig. 23.** The Nu versus  $10^4 \leq Ra \leq 10^5$  along the left vertical hot wall: continuous line (hexagonal cavity), dashed (octagonal cavity)

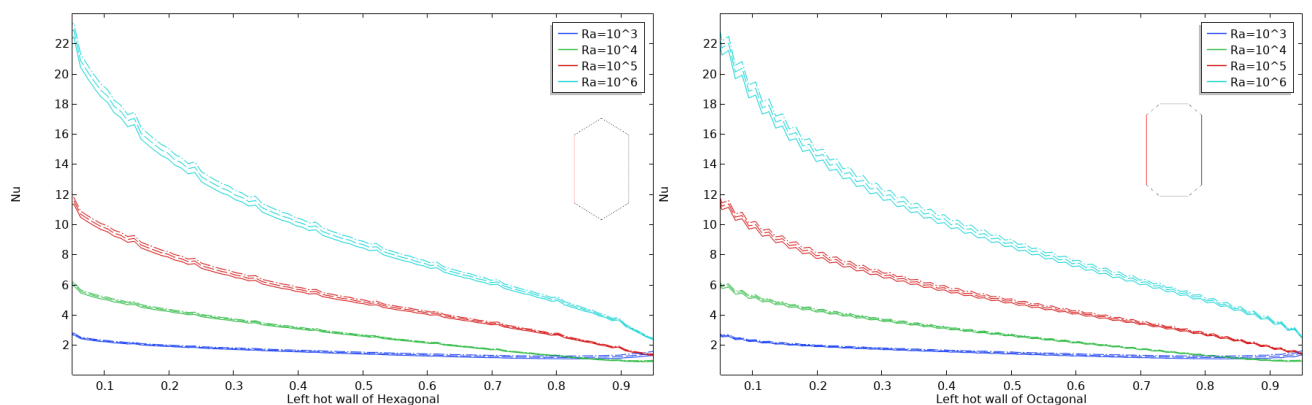


**Fig. 24.** The Nu versus the left vertical hot wall: continuous line ( $\phi=0.01$ ), dashed line ( $\phi=0.03$ ), dashed dotted line ( $\phi=0.05$ )

## 6. Conclusions

Regardless of the usual results of the effect of the solid volume fraction and the Rayleigh number effects on the laminar natural convection inside cavities. The key new findings for the unique shape hexagonal and octagonal cavities are

- i. The variation in the velocities (U) and (W) inside the hexagonal cavity are higher than that inside the octagonal.
- ii. For ( $\Delta\phi=0.04$  at  $Ra=10^6$ ), the hexagonal and octagonal have increase of ( $\Delta U=1.002\%$ ) and ( $\Delta U=0.8\%$ ) while decreases ( $\Delta W=0.15\%$ ) and ( $\Delta W=0.02\%$ ) respectively.
- iii. At the lower left part (close to the hot wall) of both cavities, the temperature value is higher for higher solid volume fraction and lower Ra, reverse observation appears at the upper right part (close to the cold wall).
- iv. Nu for the octagonal cavity is higher than the hexagonal cavity although of the same volume of cavities and the same shape, dimensions and orientations of the hot and cold walls.
- v. The increase in Nu of the octagonal cavity over the hexagonal cavity for all solid volume fractions is constant which is about ( $\Delta Nu = 0.6\%, 0.8\%, 0.7\%, 0.3\%$ ) for ( $Ra = 10^3, 10^4, 10^5, 10^6$ ) in respect.

## References

- [1] Mebarek-Oudina, F., and I. Chabani. "Review on nano-fluids applications and heat transfer enhancement techniques in different enclosures." *Journal of Nanofluids* 11, no. 2 (2022): 155-168. <https://doi.org/10.1166/jon.2022.1834>
- [2] Rostami, Sara, Saeed Aghakhani, Ahmad Hajatzadeh Pordanjani, Masoud Afrand, Goshtasp Cheraghian, Hakan F. Oztop, and Mostafa Safdari Shadloo. "A review on the control parameters of natural convection in different shaped cavities with and without nanofluid." *Processes* 8, no. 9 (2020): 1011. <https://doi.org/10.3390/pr8091011>
- [3] Giwa, S. O., M. Sharifpur, M. H. Ahmadi, and J. P. Meyer. "A review of magnetic field influence on natural convection heat transfer performance of nanofluids in square cavities." *Journal of Thermal Analysis and Calorimetry* 145 (2021): 2581-2623. <https://doi.org/10.1007/s10973-020-09832-3>
- [4] Öztop, Hakan F., Patrice Estellé, Wei-Mon Yan, Khaled Al-Salem, Jamel Orfi, and Omid Mahian. "A brief review of natural convection in enclosures under localized heating with and without nanofluids." *International Communications in Heat and Mass Transfer* 60 (2015): 37-44. <https://doi.org/10.1016/j.icheatmasstransfer.2014.11.001>
- [5] Das, Debayan, Monisha Roy, and Tanmay Basak. "Studies on natural convection within enclosures of various (non-square) shapes-A review." *International Journal of Heat and Mass Transfer* 106 (2017): 356-406. <https://doi.org/10.1016/j.ijheatmasstransfer.2016.08.034>
- [6] Baïri, Abderrahmane, Esther Zarco-Pernia, and J-M. García De María. "A review on natural convection in enclosures for engineering applications. The particular case of the parallelogrammic diode cavity." *Applied Thermal Engineering* 63, no. 1 (2014): 304-322. <https://doi.org/10.1016/j.applthermaleng.2013.10.065>
- [7] Ayed, Sadoon K., Atheer Raheem Al Guboori, Hasanen Mohammed Hussain, and Laith Jaafer Habeeb. "Review on enhancement of natural convection heat transfer inside enclosure." *Journal of Mechanical Engineering Research and Developments* 44, no. 1 (2021): 123-134.
- [8] Hussein, Ahmed Kadhim, Mohamed M. Awad, Lioua Kolsi, Farshid Fathinia, and I. K. Adegun. "A comprehensive review of transient natural convection flow in enclosures." *Journal of Basic and Applied Scientific Research* 4, no. 11 (2014): 17-27.
- [9] Majdi, Hassa Sh, Ammar Abdulkadhim, and Azher M. Abed. "Numerical investigation of natural convection heat transfer in a parallelogramic enclosure having an inner circular cylinder using liquid nanofluid." *Frontiers in Heat and Mass Transfer* 12, no. 2 (2019): 1-14. <https://doi.org/10.5098/hmt.12.2>
- [10] Al-Rashed, Abdullah A. A. A., Lioua Kolsi, Karuppan Kalidasan, Emad Hasani Malekshah, Mohamed Naceur Borjini, and P. Rajesh Kanna. "Second law analysis of natural convection in a CNT-water nanofluid filled inclined 3D cavity with incorporated Ahmed body." *International Journal of Mechanical Sciences* 130 (2017): 399-415. <https://doi.org/10.1016/j.ijmecsci.2017.06.028>
- [11] Al-Rashed, Abdullah AAA, K. Kalidasan, Lioua Kolsi, Mohamed Naceur Borjini, and P. Rajesh Kanna. "Three-dimensional natural convection of CNT-water nanofluid confined in an inclined enclosure with Ahmed body." *Journal of Thermal Science and Technology* 12, no. 1 (2017): JTST0002. <https://doi.org/10.1299/jtst.2017jtst0002>
- [12] Al-Rashed, Abdullah A. A. A., Walid Hassen, Lioua Kolsi, Hakan F. Oztop, Ali J. Chamkha, and Nidal Abu-Hamdeh. "Three-dimensional analysis of natural convection in nanofluid-filled parallelogrammic enclosure opened from top and heated with square heater." *Journal of Central South University* 26, no. 5 (2019): 1077-1088. <https://doi.org/10.1007/s11771-019-4072-0>
- [13] Hussein, Ahmed Kadhim, Kolsi Lioua, Ramesh Chand, S. Sivasankaran, Rasoul Nikbakhti, Dong Li, Borjini Mohamed Naceur, and Ben Aïssia Habib. "Three-dimensional unsteady natural convection and entropy generation in an inclined cubical trapezoidal cavity with an isothermal bottom wall." *Alexandria Engineering Journal* 55, no. 2 (2016): 741-755. <https://doi.org/10.1016/j.aej.2016.01.004>
- [14] Yan, Shu-Rong, Ahmad Hajatzadeh Pordanjani, Saeed Aghakhani, Aysan Shahsavar Goldanlou, and Masoud Afrand. "Management of natural convection of nanofluids inside a square enclosure by different nano powder shapes in presence of Fins with different shapes and magnetic field effect." *Advanced Powder Technology* 31, no. 7 (2020): 2759-2777. <https://doi.org/10.1016/j.appt.2020.05.009>
- [15] Ma, Yuan, Rasul Mohebbi, M. M. Rashidi, Zhigang Yang, and Mikhail A. Sheremet. "Numerical study of MHD nanofluid natural convection in a baffled U-shaped enclosure." *International Journal of Heat and Mass Transfer* 130 (2019): 123-134. <https://doi.org/10.1016/j.ijheatmasstransfer.2018.10.072>
- [16] Chahrazed, Benseghir, and Rahal Samir. "Simulation of heat transfer in a square cavity with two fins attached to the hot wall." *Energy Procedia* 18 (2012): 1299-1306. <https://doi.org/10.1016/j.egypro.2012.05.147>
- [17] Saeid, Nawaf H. "Natural convection in a square cavity with discrete heating at the bottom with different fin shapes." *Heat Transfer Engineering* 39, no. 2 (2018): 154-161. <https://doi.org/10.1080/01457632.2017.1288053>

- [18] Asl, Alireza Keyhani, Siamak Hossainpour, M. M. Rashidi, M. A. Sheremet, and Z. Yang. "Comprehensive investigation of solid and porous fins influence on natural convection in an inclined rectangular enclosure." *International Journal of Heat and Mass Transfer* 133 (2019): 729-744. <https://doi.org/10.1016/j.ijheatmasstransfer.2018.12.156>
- [19] Siavashi, Majid, Reza Yousofvand, and Saeed Rezanejad. "Nanofluid and porous fins effect on natural convection and entropy generation of flow inside a cavity." *Advanced Powder Technology* 29, no. 1 (2018): 142-156. <https://doi.org/10.1016/j.appt.2017.10.021>
- [20] Lo, D. C. "DQ analysis of 2D and 3D natural convection in an inclined cavity using a velocity-vorticity formulation." In *Recent Advances in Technologies*. IntechOpen, 2009.
- [21] Terekhov, Viktor Ivanovich, and A. L. Ekaid. "Three-dimensional laminar convection in a parallelepiped with heating of two side walls." *High Temperature* 49 (2011): 874-880. <https://doi.org/10.1134/S0018151X11060228>
- [22] Al-Rashed, Abdullah A. A., Lioua Kolsi, Ahmed Kadhim Hussein, Walid Hassen, Mohamed Aichouni, and Mohamed Naceur Borjini. "Numerical study of three-dimensional natural convection and entropy generation in a cubical cavity with partially active vertical walls." *Case Studies in Thermal Engineering* 10 (2017): 100-110. <https://doi.org/10.1016/j.csite.2017.05.003>
- [23] Alnaqi, Abdulwahab A., Ahmed Kadhim Hussein, Lioua Kolsi, Abdullah AAA Al-Rashed, Dong Li, and Hafiz Muhammad Ali. "Computational study of natural convection and entropy generation in 3-D cavity with active lateral walls." *Thermal Science* 24, no. 3 Part B (2020): 2089-2100. <https://doi.org/10.2298/TSCI180810346A>
- [24] Safiei, Wahaizad, Md Mustafizur Rahman, Ratnakar Kulkarni, Md Noor Ariffin, and Zetty Akhtar Abd Malek. "Thermal conductivity and dynamic viscosity of nanofluids: a review." *Journal of Advanced Research in Fluid Mechanics and Thermal Sciences* 74, no. 2 (2020): 66-84. <https://doi.org/10.37934/arfmts.74.2.6684>
- [25] Murshed, S. M. Soheli, Mohsen Sharifpur, Solomon Giwa, and Josua P. Meyer. "Experimental research and development on the natural convection of suspensions of nanoparticles-a comprehensive review." *Nanomaterials* 10, no. 9 (2020): 1855. <https://doi.org/10.3390/nano10091855>
- [26] Ahmadi, Mohammad Hossein, Amin Mirlohi, Mohammad Alhuyi Nazari, and Roghayeh Ghasempour. "A review of thermal conductivity of various nanofluids." *Journal of Molecular Liquids* 265 (2018): 181-188. <https://doi.org/10.1016/j.molliq.2018.05.124>
- [27] Devendiran, Dhinesh Kumar, and Valan Arasu Amirtham. "A review on preparation, characterization, properties and applications of nanofluids." *Renewable and Sustainable Energy Reviews* 60 (2016): 21-40. <https://doi.org/10.1016/j.rser.2016.01.055>
- [28] Sidik, Nor Azwadi Che, Muhammad Mahmud Jamil, Wan Mohd Arif Aziz Japar, and Isa Muhammad Adamu. "A review on preparation methods, stability and applications of hybrid nanofluids." *Renewable and Sustainable Energy Reviews* 80 (2017): 1112-1122. <https://doi.org/10.1016/j.rser.2017.05.221>
- [29] Elfaghi, Abdulhafid M. A., Alhadi A. Abosbaia, Munir F. A. Alkibir, and Abdoulhdi A. B. Omran. "CFD Simulation of Forced Convection Heat Transfer Enhancement in Pipe Using Al<sub>2</sub>O<sub>3</sub>/Water Nanofluid." *Journal of Advanced Research in Numerical Heat Transfer* 8, no. 1 (2022): 44-49. <https://doi.org/10.37934/cfdl.14.9.118124>
- [30] Razali, Nizamuddin, Mohd Bekri Rahim, and Sri Sumarwati. "Influence of Volume Fraction of Titanium Dioxide Nanoparticles on the Thermal Performance of Wire and Tube of Domestic Refrigerator Condenser Operated with Nanofluid." *Journal of Advanced Research in Numerical Heat Transfer* 11, no. 1 (2022): 12-22.
- [31] Alkasasbeh, Hamzeh, Feras M. AlFaqih, and Abedalrahman S. Shoul. "Computational Simulation of Magneto Convection Flow of Williamson Hybrid Nanofluid with Thermal Radiation Effect." *CFD Letters* 15, no. 4 (2023): 92-105. <https://doi.org/10.37934/cfdl.15.4.92105>
- [32] Kolsi, Lioua, Emtinene Lajnef, Walid Aich, Abdulaziz Alghamdi, Mohamed Ahmed Aichouni, Mohamed Naceur Borjini, and Habib Ben Aissia. "Numerical investigation of combined buoyancy-thermocapillary convection and entropy generation in 3D cavity filled with Al<sub>2</sub>O<sub>3</sub> nanofluid." *Alexandria Engineering Journal* 56, no. 1 (2017): 71-79. <https://doi.org/10.1016/j.aej.2016.09.005>
- [33] Rahimi, Alireza, Abbas Kasaeipoor, Emad Hasani Malekshah, Mohammad Mehdi Rashidi, and Abimanyu Purusothaman. "Lattice Boltzmann simulation of 3D natural convection in a cuboid filled with KKL-model predicted nanofluid using Dual-MRT model." *International Journal of Numerical Methods for Heat & Fluid Flow* 29, no. 1 (2019): 365-387. <https://doi.org/10.1108/HFF-07-2017-0262>
- [34] Esfe, Mohammad Hemmat, Ramtin Barzegarian, and Mehdi Bahiraei. "A 3D numerical study on natural convection flow of nanofluid inside a cubical cavity equipped with porous fins using two-phase mixture model." *Advanced Powder Technology* 31, no. 6 (2020): 2480-2492. <https://doi.org/10.1016/j.appt.2020.04.012>
- [35] Timofeeva, Elena V., Alexei N. Gavrilov, James M. McCloskey, Yuriy V. Tolmachev, Samuel Sprunt, Lena M. Lopatina, and Jonathan V. Selinger. "Thermal conductivity and particle agglomeration in alumina nanofluids: experiment and theory." *Physical Review E* 76, no. 6 (2007): 061203. <https://doi.org/10.1103/PhysRevE.76.061203>

- [36] Rashad, A. M., M. M. Rashidi, Giulio Lorenzini, Sameh E. Ahmed, and Abdelraheem M. Aly. "Magnetic field and internal heat generation effects on the free convection in a rectangular cavity filled with a porous medium saturated with Cu-water nanofluid." *International Journal of Heat and Mass Transfer* 104 (2017): 878-889. <https://doi.org/10.1016/j.ijheatmasstransfer.2016.08.025>
- [37] Bouabid, Mounir, Nejb Hidouri, Mourad Magherbi, Atef Eljery, and A. Ben Brahim. "Irreversibility investigation on MHD natural convection in a square cavity for different Prandtl numbers." *World Journal of Engineering and Physical Sciences* 2, no. 4 (2014): 60-75.
- [38] Bouabid, Mounir, Nejb Hidouri, Mourad Magherbi, and Ammar Ben Brahim. "Analysis of the magnetic field effect on entropy generation at thermosolutal convection in a square cavity." *Entropy* 13, no. 5 (2011): 1034-1054. <https://doi.org/10.3390/e13051034>
- [39] Bouabid, Mounir, Mourad Magherbi, Nejb Hidouri, and Ammar Ben Brahim. "Entropy generation at natural convection in an inclined rectangular cavity." *Entropy* 13, no. 5 (2011): 1020-1033. <https://doi.org/10.3390/e13051020>
- [40] Kasaeian, Alibakhsh, Reza Daneshzarian, Omid Mahian, Lioua Kolsi, Ali J. Chamkha, Somchai Wongwises, and Ioan Pop. "Nanofluid flow and heat transfer in porous media: a review of the latest developments." *International Journal of Heat and Mass Transfer* 107 (2017): 778-791. <https://doi.org/10.1016/j.ijheatmasstransfer.2016.11.074>
- [41] Ghasemi, Kasra, and Majid Siavashi. "Lattice Boltzmann numerical simulation and entropy generation analysis of natural convection of nanofluid in a porous cavity with different linear temperature distributions on side walls." *Journal of Molecular Liquids* 233 (2017): 415-430. <https://doi.org/10.1016/j.molliq.2017.03.016>
- [42] Mejbel, Abed Isam, Ammar Abdulkadhim, Ruqaiya A. Hamzah, Hamed K. Hamzah, and Farooq H. Ali. "Natural convection heat transfer for adiabatic circular cylinder inside trapezoidal enclosure filled with nanofluid superposed porous-nanofluid layer." *FME Transactions* 48, no. 1 (2020): 82-89. <https://doi.org/10.5937/fmet2001082M>
- [43] Kolsi, Lioua, Ahmed Kadhim Hussein, Mohamed Naceur Borjini, H. A. Mohammed, and Habib Ben Aïssia. "Computational analysis of three-dimensional unsteady natural convection and entropy generation in a cubical enclosure filled with water-Al<sub>2</sub>O<sub>3</sub> nanofluid." *Arabian Journal for Science and Engineering* 39 (2014): 7483-7493. <https://doi.org/10.1007/s13369-014-1341-y>
- [44] Salari, Mahmoud, Emad Hasani Malekshah, and Mohammad Hemmat Esfe. "Three dimensional simulation of natural convection and entropy generation in an air and MWCNT/water nanofluid filled cuboid as two immiscible fluids with emphasis on the nanofluid height ratio's effects." *Journal of Molecular Liquids* 227 (2017): 223-233. <https://doi.org/10.1016/j.molliq.2016.12.004>
- [45] Salari, Mahmoud, Emad Hasani Malekshah, and Masoud Hasani Malekshah. "Three-dimensional numerical analysis of the natural convection and entropy generation of MWCNTs-H<sub>2</sub>O and air as two immiscible fluids in a rectangular cuboid with fillet corners." *Numerical Heat Transfer, Part A: Applications* 71, no. 8 (2017): 881-894. <https://doi.org/10.1080/10407782.2017.1309213>
- [46] Kolsi, Lioua, K. Kalidasan, Abdulaziz Alghamdi, Mohamed Naceur Borjini, and P. Rajesh Kanna. "Natural convection and entropy generation in a cubical cavity with twin adiabatic blocks filled by aluminum oxide-water nanofluid." *Numerical Heat Transfer, Part A: Applications* 70, no. 3 (2016): 242-259. <https://doi.org/10.1080/10407782.2016.1173478>
- [47] Kolsi, Lioua, Hakan F. Öztöp, Abdulaziz Alghamdi, Nidal Abu-Hamdeh, Mohamed Naceur Borjini, and Habib Ben Aïssia. "A computational work on a three dimensional analysis of natural convection and entropy generation in nanofluid filled enclosures with triangular solid insert at the corners." *Journal of Molecular Liquids* 218 (2016): 260-274. <https://doi.org/10.1016/j.molliq.2016.02.083>
- [48] Kolsi, Lioua, Omid Mahian, Hakan F. Öztöp, Walid Aich, Mohamed Naceur Borjini, Nidal Abu-Hamdeh, and Habib Ben Aïssia. "3D buoyancy-induced flow and entropy generation of nanofluid-filled open cavities having adiabatic diamond shaped obstacles." *Entropy* 18, no. 6 (2016): 232. <https://doi.org/10.3390/e18060232>
- [49] Kolsi, Lioua, Abdullah A. A. Alrashed, Khaled Al-Salem, Hakan F. Öztöp, and Mohamed Naceur Borjini. "Control of natural convection via inclined plate of CNT-water nanofluid in an open sided cubical enclosure under magnetic field." *International Journal of Heat and Mass Transfer* 111 (2017): 1007-1018. <https://doi.org/10.1016/j.ijheatmasstransfer.2017.04.069>
- [50] Jelodari, Iman, and Amir H. Nikseresht. "Effects of Lorentz force and induced electrical field on the thermal performance of a magnetic nanofluid-filled cubic cavity." *Journal of Molecular Liquids* 252 (2018): 296-310. <https://doi.org/10.1016/j.molliq.2017.12.143>
- [51] Moutaouakil, L. E., Mohammed Boukendil, Zaki Zrikem, and Abdelhalim Abdelbaki. "Natural convection and thermal radiation influence on nanofluids in a cubical cavity." *International Journal of Heat and Technology* 38, no. 1 (2020): 59-68. <https://doi.org/10.18280/ijht.380107>
- [52] Sannad, Mohamed, Btissam Abourida, and El Houcine Belarache. "Numerical study of the effect of the nanofluids type and the size of the heating sections on heat transfer for cooling electronic components." *Journal of Advanced*

- Research in Fluid Mechanics and Thermal Sciences* 75, no. 2 (2020): 168-184. <https://doi.org/10.37934/arfmts.75.2.168184>
- [53] Sannad, Mohamed, Abourida Btissam, and Belarche Lahoucine. "Numerical Simulation of the natural convection with presence of the nanofluids in cubical cavity." *Mathematical Problems in Engineering* 2020 (2020): 1-17. <https://doi.org/10.1155/2020/8375405>
- [54] Selimefendigil, Fatih, and Hakan F. Öztop. "Control of natural convection in a CNT-water nanofluid filled 3D cavity by using an inner T-shaped obstacle and thermoelectric cooler." *International Journal of Mechanical Sciences* 169 (2020): 105104. <https://doi.org/10.1016/j.ijmecsci.2019.105104>
- [55] Al-Rashed, Abdullah, K. Kalidasan, Lioua Kolsi, Chemseddine Maatki, Mohamed BORJINI, Mohamed Aichouni, and P. Rajesh Kanna. "Effect of magnetic field inclination on magneto-convective induced irreversibilities in a CNT-water nanofluid filled cubic cavity." *Frontiers in Heat and Mass Transfer (FHMT)* 8, no. 31 (2017). <https://doi.org/10.5098/hmt.8.31>
- [56] Bendrer, B. A. I., Aissa Abderrahmane, Sameh E. Ahmed, and Zehba AS Raizah. "3D magnetic buoyancy-driven flow of hybrid nanofluids confined wavy cubic enclosures including multi-layers and heated obstacle." *International Communications in Heat and Mass Transfer* 126 (2021): 105431. <https://doi.org/10.1016/j.icheatmasstransfer.2021.105431>
- [57] Lai, Feng-Hsiang, and Yue-Tzu Yang. "Lattice Boltzmann simulation of natural convection heat transfer of Al<sub>2</sub>O<sub>3</sub>/water nanofluids in a square enclosure." *International Journal of Thermal Sciences* 50, no. 10 (2011): 1930-1941. <https://doi.org/10.1016/j.ijthermalsci.2011.04.015>
- [58] Öztop, Hakan Fehmi, Moghtada Mobedi, Eiyad Abu-Nada, and Ioan Pop. "A heatline analysis of natural convection in a square inclined enclosure filled with a CuO nanofluid under non-uniform wall heating condition." *International Journal of Heat and Mass Transfer* 55, no. 19-20 (2012): 5076-5086. <https://doi.org/10.1016/j.ijheatmasstransfer.2012.05.007>
- [59] Abu-Nada, Eiyad, and Hakan F. Oztop. "Effects of inclination angle on natural convection in enclosures filled with Cu-water nanofluid." *International Journal of Heat and Fluid Flow* 30, no. 4 (2009): 669-678. <https://doi.org/10.1016/j.ijheatfluidflow.2009.02.001>
- [60] Tric, E., G. Labrosse, and M. Betrouni. "A first incursion into the 3D structure of natural convection of air in a differentially heated cubic cavity, from accurate numerical solutions." *International Journal of Heat and Mass Transfer* 43, no. 21 (2000): 4043-4056. [https://doi.org/10.1016/S0017-9310\(00\)00037-5](https://doi.org/10.1016/S0017-9310(00)00037-5)
- [61] Peng, Y., C. Shu, and Y. T. Chew. "A 3D incompressible thermal lattice Boltzmann model and its application to simulate natural convection in a cubic cavity." *Journal of Computational Physics* 193, no. 1 (2004): 260-274. <https://doi.org/10.1016/j.jcp.2003.08.008>
- [62] Purusothaman, A., N. Nithyadevi, H. F. Oztop, V. Divya, and K. Al-Salem. "Three dimensional numerical analysis of natural convection cooling with an array of discrete heaters embedded in nanofluid filled enclosure." *Advanced Powder Technology* 27, no. 1 (2016): 268-280. <https://doi.org/10.1016/j.apt.2015.12.012>